AN UNCONDITIONALLY STABLE, ENERGY PRESERVING METHOD FOR MAGNETOHYDRODYNAMICS

J.A. Hopman¹, D. Santos¹, J. Rigola¹ and F.X. Trias¹

¹ Heat and Mass Transfer Technological Center, Technical University of Catalonia ESEIAAT, c/Colom 11, Terrassa, 08222, Barcelona, Spain

jannes.hopman@upc.edu

Abstract

Many industrial applications, such as nuclear fusion reactor design and aeronautics, require accurate numerical simulation tools, that conserve physical properties, for magnetohydrodynamic (MHD) flows at low magnetic Reynolds numbers. The interaction between the magnetic field and the conductive fluid often results in complex flow phenomena, which require conservative discretisation schemes. These schemes minimise numerical dissipation to improve accuracy, but can lead to the checkerboard problem if applied on collocated grid arrangements, which are necessary in complex geometries. An algorithm is constructed to simulate MHD flows, which relies on the symmetrypreserving discretisation to allow minimal numerical dissipation. Moreover, it quantifies the checkerboard problem, to dynamically balance it with numerical dissipation, only when necessary. Turbulent MHD duct flow cases show the ability of the solver to generate accurate flow statistics, while mitigating checkerboarding which lead to flow laminarisation in a comparative solver. These findings establish the presented framework as a reliable and efficient approach for MHD simulations at low magnetic Reynolds numbers, particularly where collocated grid arrangements and low numerical dissipation are required.

1 Introduction

Accurate simulation tools for magnetohydrodynamic (MHD) flows at low magnetic Reynolds number are of great interest for many industrial applications, such as in the design of nuclear fusion reactors [Hoshino et al. (2011)]. Extreme circumstances created inside the reactor limit the use of experimental techniques, leaving numerical modeling as the method of choice [Abdou et al. (2001)]. The interaction of the conductive fluids with magnetic fields, leads to an opposing Lorentz force. Accurate numerical schemes which conserve physical properties such as mass, momentum, kinetic energy and charge density, are of great importance when modeling the delicate balance between the high pressure drop and the opposing Lorentz force. The opposing Lorentz force is stronger at the center of the flow, which can create quasi-two-dimensional turbulence effects at high

Reynolds numbers [Smolentsev et al. (2015)]. In these cases, conservative schemes are essential in depicting turbulent transition in space and time, since numerical dissipation greatly affects the small scale flow structures which form the basis of turbulence [Verstappen and Veldman (2003)]. The often complex geometries found in industrial applications require a collocated grid approach, which, combined with lowdissipative schemes for incompressible flows, can lead to the checkerboard problem [Trias et al. (2014)]. The problem finds its origins in the discrete collocated gradient and Laplacian operators, which are insensitive to high-frequency modes in the pressure [Hopman et al. (2025)]. This problem becomes more relevant in MHD at low magnetic Reynolds numbers, since an additional Poisson equation is formed to solve the electric potential field. In most finite volume codes, the classical Rhie-Chow interpolation and a compactstencil Laplacian operator are used to minimise the checkerboard problem at the cost of adding numerical dissipation. A low-dissipative method for MHD is developed, which quantifies the checkerboard problem and allows numerical dissipation in the solution accordingly, and thereby maintains high accuracy and unconditional stability. This numerical framework is presented in section 2. The method is tested on a turbulent duct flow benchmark case with a conductive fluid and a transverse magnetic field. Some preliminary test results are presented in section 3.

2 Numerical Framework

A fractional step method forms the basis of the numerical scheme, of which the equations are given in algorithm 1. The discretisation of the algebraic operators can be found in [Hopman et~al.~(2025)], with the physical variables given by: collocated velocity, \mathbf{u}_c , staggered velocity, \mathbf{u}_s , modified kinematic pressure $\tilde{\mathbf{p}}_c$, current density, \mathbf{J}_c , magnetic field, \mathbf{B}_c , electric potential, ϕ_c , density, ρ , and electrical conductivity, σ . The discrete operators are given by: collocated gradient, G_c . face gradient, G_c , collocated divergence, M_c , compact-stencil Laplacian, E_c , cell-to-face dot-interpolator, E_c and face-to-cell interpolator, E_c . Treatment of the temporal discretisation is left out of scope, and the temporal treatment of the con-

vective and diffusive terms are included in function $\mathcal{F}(\mathbf{u}_c, \mathbf{u}_s)$. $[\cdot]_{\times}$ gives a skew-symmetric matrix form of a vector field which enables the cell-wise cross product between two vector fields.

$\mathbf{u}_c^p = \mathcal{F}(\mathbf{u}_c, \mathbf{u}_s) - G_c ilde{\mathbf{p}}_c^p + rac{1}{ ho} [\mathbf{J}_c^n]_ imes \mathbf{B}_c^n$	(A1.1)
$L ilde{\mathbf{p}}_c'=M_c\mathbf{u}_c^p$	(A1.2)
$\mathbf{u}_s^{n+1} = \Gamma_{cs} \mathbf{u}_c^p - G \tilde{\mathbf{p}}_c'$	(A1.3)
$\mathbf{u}_c^{n+1} = \mathbf{u}_c^p - G_c \tilde{\mathbf{p}}_c'$	(A1.4)
$\tilde{\mathbf{p}}_c^{n+1} = \tilde{\mathbf{p}}_c^p + \tilde{\mathbf{p}}_c'$	(A1.5)
$\mathbf{J}_c^p = \sigma([\mathbf{u}_c^{n+1}] \times \mathbf{B}_c^n - G_c \boldsymbol{\phi}_c^p)$	(A1.6)
$Loldsymbol{\phi}_c' = M_c \mathbf{J}_c^p/\sigma$	(A1.7)
$\mathbf{J}_c^{n+1} = \Gamma_{sc}(\Gamma_{cs}\mathbf{J}_c^p - \sigma G \boldsymbol{\phi}_c')$	(A1.8)
$\boldsymbol{\phi}_c^{n+1} = \boldsymbol{\phi}_c^p + \boldsymbol{\phi}_c'$	(A1.9)

Algorithm 1: Symmetry-preserving algorithm for MHD flows

Compared to well-known hydrodynamic versions of algorithm 1, the MHD part only consists of an extra source term in the form of a Lorentz force in equation (A1.1), and equations (A1.6)-(A1.9), in which a second Poisson equation for the electromagnetic quantities is posed and solved. The definition of the face-to-cell interpolator, Γ_{sc} , in equation (A1.8) plays a crucial role in the conservation of charge density, and prevents numerical dissipation through the form of Lorentz work. In this framework, the definition is linked to the cell-to-face dot interpolator, Γ_{cs} , by:

$$\Gamma_{sc} = \Omega^{-1} \Gamma_{cs}^T \Omega_s, \tag{1}$$

with volumetric interpolation between cell-centers and faces, Γ_{cs} , to ensure unconditional stability [Santos *et al.* (2025)]. This is in contrast with the definition by [Ni *et al.* (2007)]:

$$\left[\Gamma_{sc}^{Ni}\mathbf{v}_{s}\right]_{i} = \sum_{f \in F_{f}(i)} \frac{A_{f}\left(\mathbf{r}_{f} - \mathbf{r}_{i}\right)}{\Omega_{i}} \left[\mathbf{v}_{s}\right]_{f}, \quad (2)$$

where $\mathbf{r}_f - \mathbf{r}_i$ gives the vector from cell-center i to face-center f, for which the relation given in equation (1) does not hold.

Addition of the predictor fields for p and ϕ in equations (A1.1) and (A1.6) can increase the order of the numerical errors and lower the numerical dissipation. However, setting these predictor values to the values at the previous time-step can cause checkerboarding in the solution fields. Therefore, by quantifying the checkerboard problem, a coefficient can be calculated which directly couples back to the predictor value. Thereby establishing a negative feedback mechanism which is able to dynamically balance the checkerboard problem with numerical dissipation. The predictor values in the final algorithm are defined by:

$$\boldsymbol{\alpha}_c^p = (1 - \alpha_{cb}) \, \boldsymbol{\alpha}_c^n, \tag{3}$$

where α represents the pressure or electric potential field. α_{cb} gives the quantity of checkerboarding of the respective fields, and is calculated as:

$$\alpha_{cb} = \frac{\boldsymbol{\alpha}_c^T \left(L - L_c \right) \boldsymbol{\alpha}_c}{\boldsymbol{\alpha}_c^T L \boldsymbol{\alpha}_c},\tag{4}$$

with $\alpha_{cb}=0$ if the denominator equals zero. This symmetry-preserving algorithm with dynamical treatment of the checkerboarding was compared to a method which uses equation (2) to interpolate the charge density, and which does not have the dynamical treatment of the predictor fields.

The solver is implemented in open source software OpenFOAM, and made available under *RKSymMag-Foam* at [Hopman and Frederix (2003)].

3 Results

Case description. To examine the accuracy of the proposed solver, several turbulent duct flow cases were used. Initially, a hydrodynamic square duct flow was utilised, similar to [Zhang et al. (2015)], to benchmark the solver, with $Re_{\tau} = \frac{\overline{u_{\tau}}D_{H}}{\nu} = 300$, frictional velocity $\overline{u_{\tau}} = \sqrt{\frac{\overline{\tau_w}}{\rho}}$, and wall shear stress $\overline{\tau_w}=\overline{\mu\frac{\partial u_w}{\partial_n}},$ using the dynamic viscosity $\mu.$ This value takes the velocity derivative at the wall and averages it along the perimeter of the duct. A fixed pressure gradient and cyclic boundaries in the stream-wise direction were used to drive the flow. The relation between the driving pressure gradient and the wall shear stress leads to an exact expression for the frictional Reynolds number, $Re_{\tau} = \sqrt{\frac{D_H \nabla p}{4}} \frac{D_H}{\nu}$. The dimensions of the duct are $[16D_H \times D_H \times D_H]$ in x-,yand z-direction, respectively, as used in [Blishchik et al. (2021)]. To examine MHD effects, a Reynolds bulk was fixed with a variable pressure gradient at $Re_B = \frac{U_B D_H}{r} = 5602$, corresponding to $Re_\tau \approx 360$. At this point a magnetic field was applied in the ydirection, leading to a Hartmann number of Ha = $B_y D_H \sqrt{\frac{\sigma}{\rho \nu}} = 21.2$. The Reynolds bulk was kept constant by varying the pressure gradient and keeping the mass flow rate constant, resulting in the same governing dimensionless numbers as the ones used in [Chaudhary et. al (2010), Blishchik et al. (2021)]. A schematic drawing of the case can be seen in Figure 1, in which the Hartmann walls, normal to y, are shaded to contrast with the side walls, normal to z. It proved beneficial to work with a fixed Re_B , as an increase in the Hartmann number and the resulting Lorentz force lead to suppression of turbulence, when a fixed pressure gradient was used to drive the flow. Two different electromagnetic cases were examined, Shercliff's case, with fully insulated walls, and a case with fully conductive walls. This strongly influences the flow qualities, as fully insulated walls force the current density loops to close inside the domain. This can lead to local alignment of the current density and

the magnetic field, which affects the resulting Lorentz force. This is in contrast with the fully conductive case, where the current density loops can close outside of the domain.

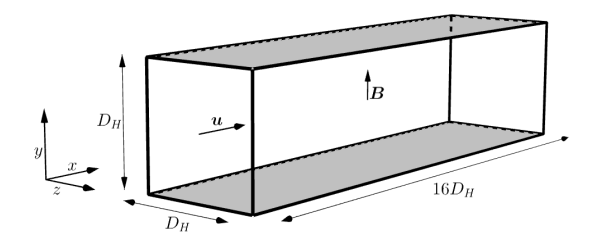


Figure 1: Schematic drawing of the duct (stream-wise dimension not to scale), with important variables indicated and Hartmann walls shaded in contrast to the side walls.

Quantification method. To quantify the accuracy of each solver, mean stream-wise velocity, the shear stressees and the turbulent kinetic energy were measured. These statistical terms are averaged in the stream-wise direction and time, and mirrored in y- and z-direction. The statistics are presented as a graph in the wall-normal direction at the center-line(s) of the duct. Finally, the checkerboard coefficient was monitored for both the pressure and electric potential field, using p_{cb} and ϕ_{cb} , respectively.

Discretisation and solvers. The newly introduced solving algorithm is denoted by SP- θ_{dy} , to indicate the symmetry-preserving (SP) discretisation with the dynamic (dy) predictor values. This solver is compared to a non-symmetry-preserving (NSP) equivalent, without the dynamic predictor values. The temporal integration was handled with the classical Runge-Kutta 3 method, as implemented in Open-FOAM by [Komen et. al (2020)] and available at [Hopman et. al (2023]. The time-step size depended on the spatial discretisation and was chosen such that the CFL number of the flow did not exceed 0.4. The cases were initialised from a pre-existing turbulent field, and developed during a transitional period, with cyclic boundaries in the stream-wise direction. The non-dimensional time units are given by $t_M =$ D_H/U_B . The case was developed for $389t_M \approx 25t_H$ and then run for an additional $1167t_M \approx 75t_H$. The approximated values are found using the frictional Reynolds number, $Re_{\tau} \approx 360$, which corresponds to the hydrodynamic duct flow at $Re_B = 5602$. Each case was run on a high quality mesh (High Mesh Q) first, which is of DNS quality, for verification of the accuracy of the solver, and to establish a reference result. Subsequently, the cases were run on a low quality mesh (Low Mesh Q) to examine the accuracy of the solvers with respect to the high quality mesh results. The mesh specifics which were used are presented in Table 1, with $\Delta i^+ = \Delta i \frac{\overline{u_\tau}}{\nu}$. Note that the cell-width at the wall, $\Delta \{y,z\}_w^+$, equals twice the distance from the wall to the first grid point at the cell-center. A stretching of the grid was applied in the wall-normal direction, following [Zhang *et al.* (2015)]:

$$d_i = \frac{L_d}{2} \left(1 + \frac{\tanh\left(g_d \frac{2i - N_d}{N_d}\right)}{\tanh\left(g_d\right)} \right), \quad (5)$$

for $i=0,1,\ldots,N_d$ and with $g_d=1.85$ and N_d the number of vertices in wall-normal direction d. On the low quality meshes, a light skew was applied in the center of the duct, with $0.1N_d \leq i \leq 0.9N_d$, to provoke checkerboarding and to see the difference between the interpolators that each solver uses. The areas close to the wall are essential for the occurrence of turbulence and are therefore not skewed.

Table 1: Different mesh characteristics used for the turbulent duct flow cases, with Δi^+ values based on $Re_{\tau}=360$. The high quality meshes are Cartesian, whereas the low quality meshes have skewed cells outside of the boundary zones. Subscript B denotes the largest cell-width, at the bulk, subscript W denotes the smallest cell-width, at the wall.

Mesh Q	N_x	$N_{\{y,z\}}$	Δx^+	$\Delta\{y,z\}_B^+$	$\Delta\{y,z\}_w^+$
Low	160	64	36.0	10.9	1.1
High	320	128	18.0	5.5	0.5

Results.

Table 2: Turbulent duct flow quantified levels of checker-boarding for p and ϕ .

		$SP-\theta_{dy}$		NSP	
Case	Mesh Q	p_{cb}	$\phi_{cb}\left(\cdot 10^{-3}\right)$	p_{cb}	$\phi_{cb}\left(\cdot 10^{-3}\right)$
Shercliff	High	0.13	0.17	-	-
,,	Low	0.50	0.64	0.89	0.61
Full Con.	High	0.12	2.75	-	-
	Low	0.49	8.33	0.87	3.62

The flow profiles for Shercliff's case are given in Figures 2–4. Since rotational symmetry is lost under the transverse magnetic field, the plots are depicted as a function of y and z. The mean stream-wise velocities, shear stresses and TKE profiles are given for in this figure. It can be seen that the NSP solver is not able to properly generate turbulence in the low quality mesh. The mean stream-wise velocity profile is closer to a parabolic shape, which is a sign of less intense turbulence. This is confirmed by the lower absolute values of the shear stresses and TKE. Although the values for the SP- θ_{dy} solver also show some disagreement with the reference result, the solver is still able to generate substantially more turbulence and give more accurate results. From Table 2, it can be seen that pressure checkerboarding might play a role in the poor accuracy results of the NSP solver, whereas the electric potential field is rather smooth for all solvers, as seen from the low values of ϕ_{cb} . However, the smooth field of ϕ_c does not necessarily mean it is not prone to checkerboarding. In fact, laminar pressure fields have shown to be more prone to checkerboarding, as the predictor value, \mathbf{p}_c^p , forms the largest part of the updated pressure, \mathbf{p}_c^{n+1} . This is because the predictor part is moved to the right-hand side of the Poisson equation, which is solved using the wide-stencil Laplacian and relies on collocated operators, allowing for disconnected neighbouring cells.

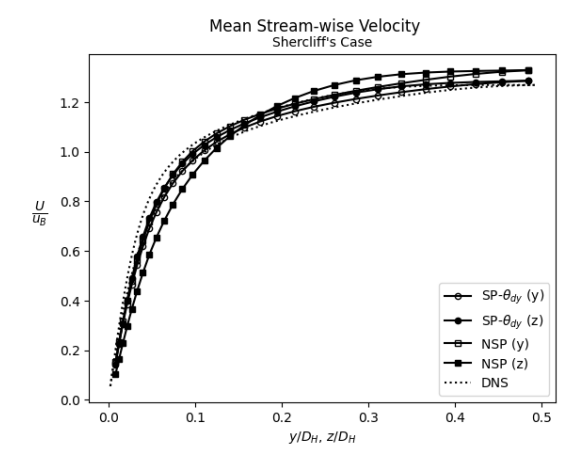


Figure 2: Mean stream-wise velocity profiles in *y*- and *z*-direction, with Shercliff boundary conditions, for each solver on the low quality mesh, compared to the DNS result.

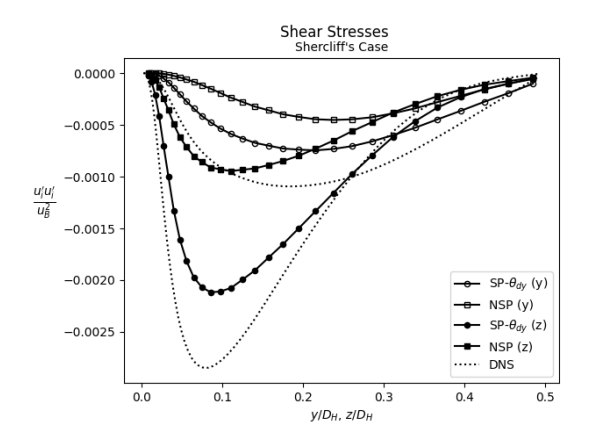


Figure 3: Shear stress profiles in *y*- and *z*-direction, with Shercliff boundary conditions, for each solver on the low quality mesh, compared to the DNS result.

The results for the fully conductive case, Figures 5–7, show that the results for the NSP solver have deteriorated further. Turbulence seems to be completely absent from the shear stresses and TKE, and the mean stream-wise flow profile deviates a lot from the reference results. The M-shape which is to be expected at this Hartmann number for laminar flow can even be seen. Table 2 shows that the case has similar lev-

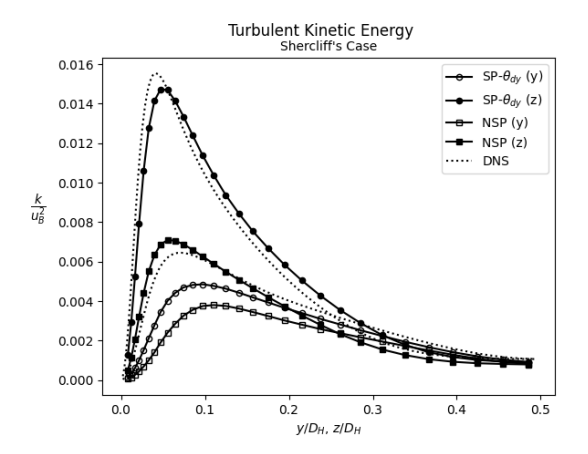


Figure 4: Turbulent kinetic energy profiles in *y*- and *z*-direction, with Shercliff boundary conditions, for each solver on the low quality mesh, compared to the DNS result.

els of checkerboarding to Shercliff's case, however is not able to fully develop turbulence. This might indicate that not just the checkerboarding, but also the non-symmetry-preserving interpolator play a role in the low accuracy results.

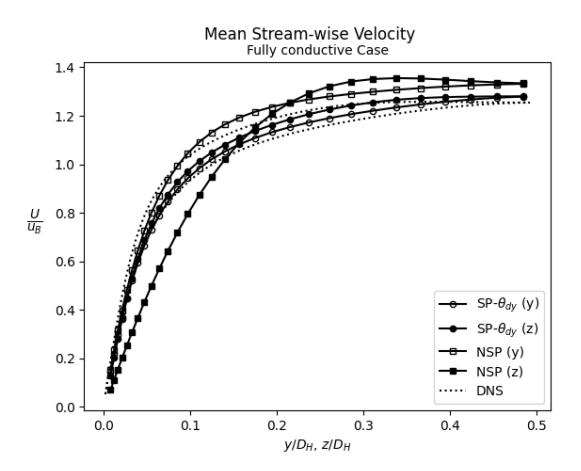


Figure 5: Mean stream-wise velocity profiles in *y*- and *z*-direction, with fully conductive boundary conditions, for each solver on the low quality mesh, compared to the DNS result.

4 Conclusions

In this work, the symmetry-preserving method is implemented for MHD flows, and extended with a dynamic method to balance checkerboarding with numerical dissipation. The symmetry-preserving method reflects the properties of the continuous operators in its discrete counterparts, making the method conservative in physical properties such as mass, momentum, kinetic energy and charge density and therefore unconditionally stable, not considering potential instability issues resulting from the temporal integra-

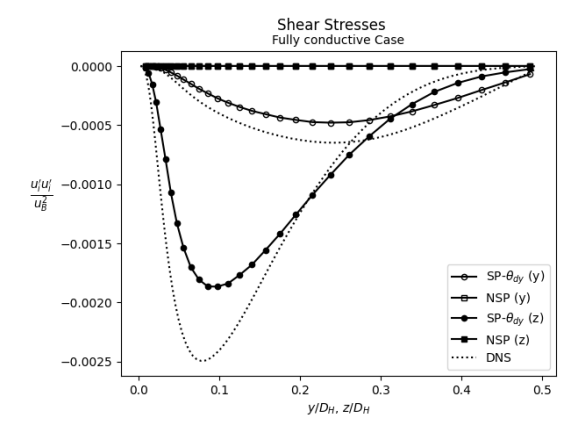


Figure 6: Shear stress profiles in *y*- and *z*-direction, with fully conductive boundary conditions, for each solver on the low quality mesh, compared to the DNS result.

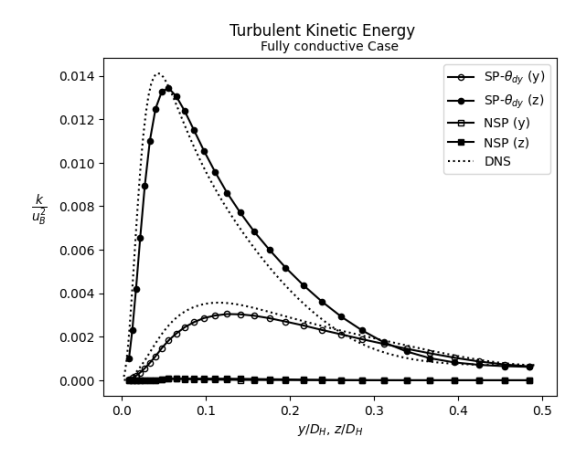


Figure 7: Turbulent kinetic energy profiles in *y*- and *z*-direction, with fully conductive boundary conditions, for each solver on the low quality mesh, compared to the DNS result.

tion method and leaving only the pressure error due to the collocated grid arrangement. On collocated grid arrangements for complex geometries, the method of interpolating variables between their staggered and collocated placements is vital in retaining this conservation to the highest degree possible. This can be done successfully, by defining a volume-weighted relation between the face-to-cell interpolator and its transpose counterpart. A second challenge when using collocated grids, is the occurrence of checkerboarding in solution fields of the Poisson equations, which occur for both pressure and electric potential in commonly used algorithms for MHD flows at low magnetic Reynolds numbers. Low numerical dissipation in combination with temporal and spatial discretisation factors can evoke checkerboarding. Allowing some numerical dissipation counter-acts the problem, however, this should be minimised as much as

possible. By quantifying the severity of the checkerboard problem during run-time, and using this value in a negative feedback mechanism through predictor fields, the checkerboard problem is mitigated only when it arises, and with minimal numerical dissipation.

The turbulent duct flow cases show the performance of the solver in a three-dimensional case in which any numerical dissipation can greatly affect the resulting flow statistics. MHD duct flow cases with insulated and conductive boundary conditions were used to study the accuracy of the solvers, by calculating the turbulent kinetic energy budgets. The results show that a non-symmetry-preserving method without any treatment for checkerboarding is not able to accurately generate the expected turbulent flow on skew meshes, in some cases resulting in a laminarised flow profile. The tendency to evoke checkerboarding on skew meshes, which can further deteriorate the flow statistics, is diminished by applying a dynamic predictor value, while at the same time offering an accurate solution

The symmetry-preserving discretisation method, as well as the checkerboard quantification method both show their usefulness in MHD flows at low magnetic Reynolds numbers. The usefulness for the dynamic electric potential predictor field was more difficult to demonstrate, however, as this field did not show much variance in the levels of checkerboarding. Test cases which are known to develop more fluctuating charge density fields could be useful for this, as they might require a more dynamically changing electric potential field, which could be more prone to the checkerboard problem. Examining this, alongside other possible applications and feed-back mechanisms of the checkerboard coefficient will be the focus of future work.

Acknowledgements This work is supported by the SIMEX project (PID2022-142174OB-I00) of *Ministerio de Ciencia e Innovación*, Spain. J.A.H. is supported by the FI AGAUR-Generalitat de Catalunya fellowship (2023 FI_B1 00204), financed and extended by *Universitat Politècnica de Catalunya* and *Banc Santander*. The numerical experiments have been conducted on the Marenostrum5 supercomputer at the *Barcelona Supercomputing Center* under the project IM-2024-3-0019. The authors thankfully acknowledge these institutions.

References

Abdou, M. A., Ying, A., Morley, N., Gulec, K., Smolentsev, S., Kotschenreuther, M., Malang, S., Zinkle, S., Rognlien, T., Fogarty, P., Nelson, B., Nygren, R., McCarthy, K., Youssef, M. Z., Ghoniem, N., Sze, D., Wong, C., Sawan, M., Khater, H., Woolley, R., Mattas, R., Moir, R., Sharafat, S., Brooks, J., Hassanein, A., Petti, D., Tillack, M., Ulrickson, M., and Uchimoto, T. (2001), On the exploration of innovative concepts for fusion chamber technology, *Fusion Eng. Des.*, Vol. 54, No. 2, pp. 181–247.

- Blishchik, A., van der Lans, M., Kenjeres, S. (2021), An extensive numerical benchmark of the various magnetohydrodynamic flows, *Int. J. Heat Fluid Flow*, Vol. 90, 108800.
- Chaudhary, R., Vanka, S. P., Thomas, B. G. (2010), Direct numerical simulations of magnetic field effects on turbulent flow in a square duct, *Phys. Fluids*, Vol. 22, No. 7, pp. 1–15.
- Hopman, J. A., Frederix, E. M. A., RKSymFoam GitHub page (2023), URL https://github.com/janneshopman/RKSymFoam
- Hopman, J. A., Santos, D., Alsalti-Baldellou, A., Rigola, J., and Trias, F. X. (2025), Quantifying the checkerboard problem to reduce numerical dissipation, *J. Comput. Phys.*, Vol. 521, p. 113537.
- Hoshino, T., Kato, K., Natori, Y., Oikawa, F., Nakano, N., Nakamura, M., Sasaki, K., Suzuki, A., Terai, T., and Tatenuma, K. (2011), Development of advanced tritium breeding material with added lithium for ITER-TBM, *J. Nucl. Mater.*, Vol. 417, No. 1-3, pp. 684–687.
- Komen, E. M. J., Frederix, E. M. A., Coppen, T. H. J., D'Alessandro, V., Kuerten, J. G. M. (2020), Analysis of the numerical dissipation rate of different Runge–Kutta and velocity interpolation methods in an unstructured collocated finite volume method in OpenFOAM, *Comput. Phys. Commun.*
- Ni, M. J., Munipalli, R., Morley, N. B., Huang, P., and Abdou, M. A. (2007), A current density conservative scheme for incompressible MHD flows at a low magnetic Reynolds number. Part I: On a rectangular collocated grid system, *J. Comput. Phys.*, Vol. 227, No. 1, pp. 174–204.
- Santos, D., Hopman, J. A., Pérez-Segarra, C. D., and Trias, F. X. (2025), On a symmetry-preserving unconditionally stable projection method on collocated unstructured grids for incompressible flows, *J. Comput. Phys.*, Vol. 523, p. 113631.
- Sherclif, J. A. (1953), Steady motion of conducting fluids in pipes under transverse magnetic fields, *Math. Proc. Camb. Philos. Soc.* Vol. 49, No. 1, pp. 136-144.
- Smolentsev, S., Badia, S., Bhattacharyay, R., Bühler, L., Chen, L., Huang, Q., Jin, H. G., Krasnov, D., Lee, D. W., Les Valls, E. M. De, Mistrangelo, C., Munipalli, R., Ni, M. J., Pashkevich, D., Patel, A., Pulugundla, G., Satyamurthy, P., Snegirev, A., Sviridov, V., Swain, P., Zhou, T., and Zikanov, O. (2015), An approach to verification and validation of MHD codes for fusion applications, *Fusion Eng. Des.*, Vol. 100, pp. 65–72.
- Trias, F. X., Lehmkuhl, O., Oliva, A., Pérez-Segarra, C. D., and Verstappen, R. W. (2014), Symmetry-preserving discretization of Navier–Stokes equations on collocated unstructured grids, *J. Comput. Phys.*, Vol. 258, pp. 246–267.
- Verstappen, R. W., and Veldman, A. E. (2003), Symmetry-preserving discretization of turbulent flow, *J. Comput. Phys.*, Vol. 187, No. 1, pp. 343–368.
- Zhang, H. Trias, F. X., Gorobets, A., Tan, Y., Oliva, A. (2015), Direct numerical simulation of a fully developed turbulent square duct flow up to $Re_{\tau}=1200$, *Int. J. Heat Fluid Flow*, Vol. 54, pp. 258-267.